Hindawi
Shock and Vibration
Volume 2021, Article ID 6801821, 18 pages
https://doi.org/10.1155/2021/6801821

Research Article

Theoretical and Experimental Study of the Pounding Response for Adjacent Inelastic MDOF Structures Based on Dimensional Analysis

Qiaoyun Wu,[1,2] Ziliang Liu,[1] Tao Wang,[1] and Xuyong Chen [1]

[1]*School of Civil Engineering and Architecture, Wuhan Institute of Technology, Wuhan 430073, China*
[2]*State Key Laboratory of Geomechanics and Geotechnical Engineering, Institute of Rock and Soil Mechanics, Chinese Academy of Sciences, Wuhan 430071, China*

Correspondence should be addressed to Xuyong Chen; hyhwqy@163.com

Received 7 June 2021; Accepted 7 August 2021; Published 20 September 2021

Academic Editor: Kaiming Bi

Dimensional analysis is applied to study the pounding response of two inelastic multidegree of freedom (MDOF) structures under simplified earthquake excitation. The forces and deformations of the collision processes are simulated by adopting the improved Kelvin pounding model. The inelastic characteristics of MDOF structures are described by the bilinear interstory resistance model, and the representations of dimensionless impact force and the dimensionless motion equation in the pounding process are derived. On the basis of the above-mentioned theoretical deduction, the superiority of the improved Kelvin model is verified by comparing the impact response of the improved Kelvin model and the Kelvin model. Finally, the validity of the proposed theoretical method is further proved by the comparison between results from the shaking table tests of adjacent four-story and three-story steel frame structures and the corresponding numerical results obtained by the MATLAB program.

1. Introduction

The past decades have witnessed numerous earthquake disasters, causing a great number of casualties and tremendous property losses [1–4]. During earthquakes, a great number of adjacent structures suffered severe damage owing to the induced structural pounding effects, which have been recorded in investigations of the Mexico earthquake of 1985 [5], the ChiChi earthquake of 1999 [6], the Wenchuan earthquake of 2008 [7], the earthquakes in Iraq of 2017 [8], and so on.

To this end, the pounding responses of adjacent multidegree of freedom (MDOF) structures have recently aroused the interests of many researchers including Maison and Kasai [9], Anagnostopoulos and Spiliopoulos [10], Mahmoud and Jankowshi [11], and Jankowshi [12]. It is found that the pounding between adjacent constructions beneath seismic excitation is associated with the characteristics of ground motions, which are also additionally affected by the characteristics of the adjacent structures. Structural collision is a higher-order nonlinear phenomenon affected by multiple parameters, and therefore the fundamental situation in analyzing the pounding responses of adjacent constructions underneath seismic excitations has to address plenty of parameters [13]. Dimensional analysis [14] with fewer dimensionless Π parameters can reduce the number of parameters while at the same time preserving the basic behaviors of the adjacent structural collision responses.

Makris and Black [15, 16] were the first to study the response of structures under earthquake excitations using a dimensionless method. Thereby, dimensional analysis was welcomed by many scholars in studying the impact of adjacent elastic constructions. Zhang and Tang [17] investigated the effect of the soil-structure interaction on the structure underneath earthquake ground motion constructions using dimensional analysis. Dimitrakopoulos et al. [18–20] analyzed the pounding response between multiple SDOF constructions via a dimensionless method.

The pounding of structures with fewer dimensionless parameters Π is described by using Buckingham Π, in which the number of parameters that govern structural collision responses is significantly reduced. Zhai et al. [13] combined the dimensionless method with the contact element method to study the pounding responses between a single elastic oscillator and an inflexible barrier, in which the Kelvin model is employed to simulate the impact forces. Furthermore, descriptions of the forces and deformations of structures during the contact phase are written in the real-time domain. Wu et al. [21] chose a more accurate impact model, the modified Kelvin model [22], to study collisions between an elastic SDOF structure and a rigid body, overcoming the disadvantage of the Kelvin impact model and revealing the rules of structural pounding. In the above-mentioned research, adjacent structures are mostly simplified into linear SDOF structures. Nevertheless, poundings of adjacent structures are nonlinear problems, which may occur at each story of adjacent structures under earthquake excitations. Therefore, it is more realistic to model the adjacent structures as nonlinear MDOF structural models when studying the pounding response.

In this paper, the pounding response of two inelastic MDOF constructions undergoing simplified earthquake excitations is investigated by using the dimensional analysis and an improved Kelvin model. The inelastic characteristics of the MDOF structures are simulated by using the bilinear interstory resistance model [23], and MATLAB is used to deduce the expression for the dimensionless pounding force and the dimensionless equation of motion in the pounding process. The calculation results are compared to the corresponding results yielded by the Kelvin pounding model. Lastly, the shaking table tests of adjacent steel frame structures are performed, whose results are compared with the numerical simulations in order to verify the correctness and effectiveness of the proposed method.

2. Computational Models and the Dimensionless Equation of Motion

2.1. Impact Analytical Model. The pounding force generated during the collision of two adjacent inelastic MDOF structures is simulated by using an improved Kelvin pounding analytical model. The improved Kelvin analytical model is shown in Figure 1, and the pounding force can be expressed as

$$F = \overline{k}\delta(t) + \overline{c}\dot{\delta}(t), \tag{1}$$

where $\overline{k}$ is the contact unit stiffness coefficient and $\delta(t)$ and $\dot{\delta}(t)$ are the relative penetrating displacement and velocity for two objects in pounding, respectively. The damping coefficient $\overline{c}$ can be expressed as follows:

$$\overline{c} = \overline{\xi}\delta(t), \tag{2}$$

in which the damping constant $\overline{\xi}$ is

$$\overline{\xi} = \frac{3\overline{k}(1-e)}{2e(V_1 - V_2)}. \tag{3}$$

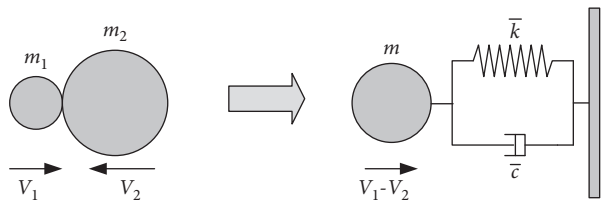

Figure 1: Improved Kelvin analytical model.

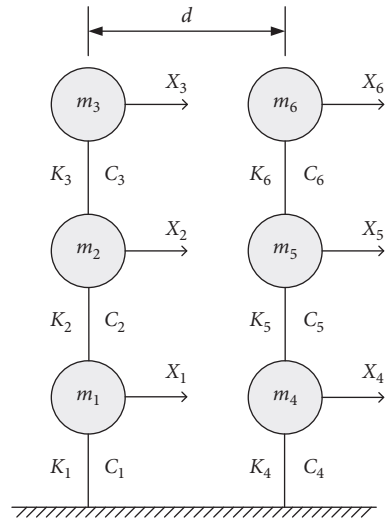

Figure 2: Adjacent MDOF pounding models.

Here, the coefficient of restitution is represented by e (an elastic pounding without energy loss is implied by $e = 1$ and complete plastic pounding is implied by $e = 0$). V_1 and V_2 indicate the velocities at which two objects collide.

Equations (1)–(3) show that the time-varying damping coefficients $\overline{c}$ have overcome the theoretical shortcomings of the Kelvin model, which involve the uniform energy loss in the contact and rebound stages of pounding, including the pounding force at the beginning of the collision and the pulling force during the rebound phase of the collision.

2.2. Equation of Motion. The adjacent three-story structures are used to illustrate the calculation model of seismic pounding (see Figure 2). As can be seen in Figure 2, the mass, stiffness, and damping coefficient of the left structure for each story are m_i, $(i = 1, 2, 3)$, K_i, $(i = 1, 2, 3)$, and C_i, $(i = 1, 2, 3)$, respectively. The mass, stiffness, and damping coefficient of the right structure for each story are m_j $(j = 1, 2, 3)$, K_j $(j = 1, 2, 3)$, and C_j $(j = 1, 2, 3)$, respectively. The original interval in the middle of the adjacent structures is d. For the study of structural nonlinearity, the constitutive relationship of the structures is simulated by using the bilinear interstory resistance model [24].

Only the acceleration amplitude and angular frequency of ground motion are required to study the seismic pounding responses of adjacent inelastic MDOF structures by using the dimensional analysis method. Consequently,

the seismic excitation can be simulated with a simplified model. Two models are used to simplify the simulations of the ground motion, which are the harmonic and pulse excitation models [25]. The ground motion excitation is assumed to be sinusoidal excitation in this paper. The acceleration amplitude is represented by a_p, and the circular frequency is represented by ω_p.

Under sinusoidal excitation, the equations of motion for the adjacent inelastic MDOF structures are

$$\mathbf{M}\ddot{\mathbf{X}}(t) + \mathbf{C}\dot{\mathbf{X}}(t) + \mathbf{F_s}(t) + \mathbf{F_p}(t) = -\mathbf{M}\ddot{\mathbf{X}}_\mathbf{g}(t), \tag{4a}$$

$$\dot{\mathbf{X}}(t) = \begin{bmatrix} \dot{X}_1(t) \\ \dot{X}_2(t) \\ \dot{X}_3(t) \\ \dot{X}_4(t) \\ \dot{X}_5(t) \\ \dot{X}_6(t) \end{bmatrix},$$

$$\ddot{\mathbf{X}}(t) = \begin{bmatrix} \ddot{X}_1(t) \\ \ddot{X}_2(t) \\ \ddot{X}_3(t) \\ \ddot{X}_4(t) \\ \ddot{X}_5(t) \\ \ddot{X}_6(t) \end{bmatrix}, \tag{4b}$$

$$\ddot{\mathbf{X}}_\mathbf{g}(t) = \begin{bmatrix} \ddot{X}_g(t) \\ \ddot{X}_g(t) \\ \ddot{X}_g(t) \\ \ddot{X}_g(t) \\ \ddot{X}_g(t) \\ \ddot{X}_g(t) \end{bmatrix},$$

$$\mathbf{M} = \begin{bmatrix} m_1 & & & & & \\ & m_2 & & & & \\ & & m_3 & & & \\ & & & m_4 & & \\ & & & & m_5 & \\ & & & & & m_6 \end{bmatrix}, \tag{4c}$$

$$\mathbf{F_s}(t) = \begin{bmatrix} F_{s1}(t) - F_{s2}(t) \\ F_{s2}(t) - F_{s3}(t) \\ F_{s3}(t) \\ F_{s4}(t) - F_{s5}(t) \\ F_{s5}(t) - F_{s6}(t) \\ F_{s6}(t) \end{bmatrix},$$

$$\mathbf{F_p}(t) = \begin{bmatrix} F_{p14}(t) \\ F_{p25}(t) \\ F_{p36}(t) \\ -F_{p14}(t) \\ -F_{p25}(t) \\ -F_{p36}(t) \end{bmatrix}, \tag{4d}$$

where $\ddot{X}_g(t)$ is the acceleration and $\ddot{X}_g(t) = a_p \sin(\omega_p t)$. $X_i(t)$, $\dot{X}_i(t)$, $\ddot{X}_i(t)$ $(i = 1, \ldots, 6)$ are the displacement, velocity, and acceleration responses of each story for adjacent structures at different times t, respectively. $F_{si}(t)$ indicates the inelastic story shear force at different times t. The incremental form of the inelastic resistance is $\Delta F_{si}(t) = K_i(t) \cdot \Delta X_i$ $(i = 1, \ldots, 6)$, in which ΔX_i is the story drift, K_i is the stiffness of the structure, and it is related to the yielding displacement u_{yi} of each structure (u_{ya} for the left structure and u_{yb} for the right structure). $\mathbf{M}$ is the matrix of the structural mass and $\mathbf{F_p}(t)$ is the matrix of the pounding force. The damping matrix $\mathbf{C}$ is the Rayleigh damping matrix, expressed as

$$\mathbf{C} = \begin{bmatrix} \mathrm{diag}[a_0]_{3\times3} & 0 \\ 0 & \mathrm{diag}[a_{0r}]_{3\times3} \end{bmatrix}\mathbf{M} + \begin{bmatrix} \mathrm{diag}[a_1]_{3\times3} & 0 \\ 0 & \mathrm{diag}[a_{1r}]_{3\times3} \end{bmatrix}\mathbf{K}, \tag{5a}$$

$$\mathbf{K} = \begin{bmatrix} K_1(t) + K_2(t) & -K_2(t) & 0 & & & \\ -K_2(t) & K_2(t) + K_3(t) & -K_3(t) & & 0 & \\ 0 & -K_3(t) & K_3(t) & & & \\ & & & K_4(t) + K_5(t) & -K_5(t) & 0 \\ & 0 & & -K_5(t) & K_5(t) + K_6(t) & -K_6(t) \\ & & & 0 & -K_6(t) & K_6(t) \end{bmatrix}, \tag{5b}$$

where

$$a_0 = \frac{2\xi\omega_{1a}\omega_{2a}}{\omega_{1a}+\omega_{2a}},$$
$$a_{0r} = \frac{2\xi\omega_{1b}\omega_{2b}}{\omega_{1b}+\omega_{2b}}, \quad (5c)$$
$$a_1 = \frac{2\xi}{\omega_{1a}+\omega_{2a}}.$$

In equation (5c), ω_{1a} is the angular frequencies of the first and ω_{2a} is second modes for the left structure; ω_{1b} is the angular frequencies of the first and ω_{2b} is second modes for the right structure, respectively; and the angular frequency ω can be obtained by solving $|\mathbf{K}-\mathbf{M}\omega^2| = 0$. $\xi = 0.05$ is the structural damping ratio assigned to the first two modes.

In this paper, the mass of each floor for the left structure and right structure is assumed to be equal, that is, $m_i = m_a (i = 1, 2, 3)$ and $m_j = m_b (j = 4, 5, 6)$. In addition, the stiffness of each floor for the left and right structures is assumed to be equal, that is, $K_i(t) = K_a$ $(i = 1, 2, 3)$ and $K_j(t) = K_b = \mu K_a (j = 4, 5, 6)$ during the elastic stage. μ is the stiffness ratio of the right structure story to the left structure story $(\mu = (K_a/K_b))$. During the plastic stage, the stiffness of each story for the left structure and right structure is $K_i(t) = \alpha K_a$ and $K_j(t) = \alpha K_b$, respectively, where α is the postyielding stiffness ratio.

According to the above assumptions and the physical quantity characterizing the energy scale of excitation l_e $(l_e = (a_p/\omega_p^2)$ with the dimensionless expression of $[L])$ proposed by Makris and Black [15, 16], the mass m_b of each floor, the amplitude $a_p (m/s^2)$, and the circular frequency $\omega_p (s^{-1})$ of the sinusoidal excitation of the right MDOF structure are selected as the basic quantity. And, the following quantities are rewritten:

$$t = \frac{\tau}{\omega_p},$$
$$X_i(t) = x_i(\tau)\cdot l_e = \frac{x_i(\tau)\cdot a_p}{\omega_p^2},$$
$$\dot{X}_i(t) = \frac{\dot{x}_i(\tau)\cdot a_p}{\omega_p}, \quad (6)$$
$$\ddot{X}_i(t) = \ddot{x}_i(\tau)\cdot a_p,$$

where τ is the dimensionless movement time. $x_i(\tau)$, $\dot{x}_i(\tau)$, $\ddot{x}_i(\tau)(i = 1, 2)$ are the relative displacement, relative velocity, and relative acceleration of each floor for the two structures, respectively.

Substituting equation (6) into equation (4a), the dimensionless equation of motion for adjacent inelastic MDOF structures can be obtained as

$$\mathbf{m}\ddot{\mathbf{x}}(\boldsymbol{\tau}) + \frac{\mathbf{C}}{m_b\omega_p}\dot{\mathbf{x}}(\boldsymbol{\tau}) + \frac{\mathbf{F_s}}{m_b\omega_p} + \frac{\mathbf{F_p}}{m_b\omega_p} = -\ddot{\mathbf{x}}_\mathbf{g}(\boldsymbol{\tau}), \quad (7a)$$

where

$$\mathbf{m} = \begin{bmatrix} \frac{m_a}{m_b} & & & & & \\ & \frac{m_a}{m_b} & & & & \\ & & \frac{m_a}{m_b} & & & \\ & & & 1 & & \\ & & & & 1 & \\ & & & & & 1 \end{bmatrix}, \quad (7b)$$

$$\dot{\mathbf{x}}(\boldsymbol{\tau}) = \begin{bmatrix} \dot{x}_1(\tau) \\ \dot{x}_2(\tau) \\ \dot{x}_3(\tau) \\ \dot{x}_4(\tau) \\ \dot{x}_5(\tau) \\ \dot{x}_6(\tau) \end{bmatrix},$$
$$\ddot{\mathbf{x}}(\boldsymbol{\tau}) = \begin{bmatrix} \ddot{x}_1(\tau) \\ \ddot{x}_2(\tau) \\ \ddot{x}_3(\tau) \\ \ddot{x}_4(\tau) \\ \ddot{x}_5(\tau) \\ \ddot{x}_6(\tau) \end{bmatrix}, \quad (7c)$$
$$\ddot{\mathbf{x}}_\mathbf{g}(\boldsymbol{\tau}) = \begin{bmatrix} \sin\tau \\ \sin\tau \\ \sin\tau \\ \sin\tau \\ \sin\tau \\ \sin\tau \end{bmatrix}.$$

By using the definition of the modified Kelvin pounding model [22] as mentioned in equation (1), the following conclusions are obtained.

When $x_i - x_j > (d/l_e)$, pounding occurs, and the expression of the pounding force is

$$F_{pij} = \frac{m_a m_b}{m_a+m_b}\overline{\omega}^2\left(x_i - x_j - \frac{d}{l_e}\right)\cdot\frac{a_p}{\omega_p^2} + \frac{3(1-e)}{2e\left(V_i - V_j\right)}\cdot\frac{m_a m_b}{m_a+m_b}\overline{\omega}^2\left(\dot{x}_i - \dot{x}_j\right)\cdot\frac{a_p}{\omega_p}\left(x_i - x_j - \frac{d}{l_e}\right)\cdot\frac{a_p}{\omega_p^2}. \quad (8a)$$

When $x_1 - x_2 < d/l_e$, no pounding occurs, and the pounding force can be expressed as

$$F_{pij} = 0. \tag{8b}$$

Substituting equation (6) into equation (8a), when pounding occurs, the dimensionless pounding force can be obtained:

$$\frac{F_{pij}}{m_b a_p} = \frac{(m_a/m_b)}{(m_a/m_b)+1}\left[\left(\frac{\overline{\omega}}{\omega_p}\right)^2 \cdot \left(x_i - x_j - \frac{d}{l_e}\right) + \frac{3(1-e)}{2e} \cdot \frac{1}{v_i - v_j} \cdot \left(\frac{\overline{\omega}}{\omega_p}\right)^2 \cdot \left(\dot{x}_i - \dot{x}_j\right) \cdot \left(x_i - x_j - \frac{d}{l_e}\right)\right], \tag{8c}$$

where v_1 and v_2 are the dimensionless velocities ($v = V \cdot (\omega_p/a_p)$) when pounding occurs between the left and right structures, respectively. $\overline{\omega}$ is the angular frequency of the contact element, and $\overline{\omega} = \sqrt{\beta(m_a + m_b)/m_a m_b}$. β is the stiffness of the contact element.

Substituting equation (6) into the damping matrix and the stiffness matrix as shown in equations (5a) and (5b), the dimensionless damping matrix and stiffness matrix can be obtained as

$$\frac{\mathbf{C}}{m_b \omega_p} = \begin{bmatrix} \mathrm{diag}\left[\frac{a_0}{\omega_p}\right]_{3\times3} & 0 \\ 0 & \mathrm{diag}\left[\frac{a_{0r}}{\omega_p}\right]_{3\times3} \end{bmatrix} \mathbf{m} + \begin{bmatrix} \mathrm{diag}\left[a_1 \omega_p\right]_{3\times3} & 0 \\ 0 & \mathrm{diag}\left[a_{1r} \omega_p\right]_{3\times3} \end{bmatrix} \frac{\mathbf{K}}{m_b \omega_p^2}, \tag{9a}$$

$$\frac{\mathbf{K}}{m_b \omega_p^2} = \begin{bmatrix} \frac{2K_a(t)}{m_b\omega_p^2} & -\frac{K_a(t)}{m_b\omega_p^2} & 0 & & & \\ -\frac{K_a(t)}{m_b\omega_p^2} & \frac{2K_a(t)}{m_b\omega_p^2} & -\frac{K_a(t)}{m_b\omega_p^2} & & 0 & \\ 0 & -\frac{K_a(t)}{m_b\omega_p^2} & \frac{K_a(t)}{m_b\omega_p^2} & & & \\ & & & \frac{2\mu K_a(t)}{m_b\omega_p^2} & -\frac{\mu K_a(t)}{m_b\omega_p^2} & 0 \\ & 0 & & -\frac{\mu K_a(t)}{m_b\omega_p^2} & \frac{2\mu K_a(t)}{m_b\omega_p^2} & -\frac{\mu K_a(t)}{m_b\omega_p^2} \\ & & & 0 & -\frac{\mu K_a(t)}{m_b\omega_p^2} & \frac{\mu K_a(t)}{m_b\omega_p^2} \end{bmatrix}, \tag{9b}$$

where

$$\frac{a_0}{\omega_p} = \frac{2\xi\left(\omega_{1a}/\omega_p\right)\left(\omega_{2a}/\omega_p\right)}{\left(\omega_{1a}/\omega_p\right)+\left(\omega_{2a}/\omega_p\right)},$$

$$\frac{a_{0r}}{\omega_p} = \frac{2\xi\left(\omega_{1b}/\omega_p\right)\left(\omega_{2b}/\omega_p\right)}{\left(\omega_{1b}/\omega_p\right)+\left(\omega_{2b}/\omega_p\right)},$$

$$a_1\omega_p = \frac{2\xi}{\left(\omega_{1a}/\omega_p\right)+\left(\omega_{2a}/\omega_p\right)}, \tag{9c}$$

$$a_{1r}\omega_p = \frac{2\xi}{\left(\omega_{1b}/\omega_p\right)+\left(\omega_{2b}/\omega_p\right)}.$$

The matrix of the dimensionless inelastic resistance $\mathbf{F_s}/m_b a_p$ is related to the dimensionless story shear force of $F_{si}/m_b a_p$. Because both adjacent structures are inelastic and $\Delta F_{si}/m_b a_p = K_i(t)\cdot\Delta x_i/m_b a_p$, the dimensionless inelastic resisting force matrix $\mathbf{F_s}/m_b a_p$ is relevant to the dimensionless story stiffness $K_i(t)/m_b a_p$, dimensionless yield displacement u_y/l_e, and postyielding stiffness ratio α.

2.3. Dimensionless Equation of Motion Based on the Buckingham Π Theorem. On the basis of the Π theorem and the equation of motion of the pounding between two inelastic MDOF structures obtained above, the pounding reaction of two inelastic MDOF structures is characterized by the peak displacement $X_{\max}$ and peak velocity $\dot{X}_{\max}$ of the stories of the structures. The parameters controlling the pounding response are the masses m_a and m_b, the stiffness K_a of the left structure, the stiffness ratio μ ($\mu = (K_a/K_b)$) measured from the right to left structure, the yield displacements u_{y1} and u_{y2}, the damping ratio ξ, the initial spacing d between the adjacent inelastic MDOF structures, the postyielding stiffness ratio α, the recovery coefficient e of the contact element, the angular frequency $\overline{\omega}$, the amplitude a_p, and the angular frequency ω_p of the sinusoidal excitation.

The expression of the pounding response function of the two inelastic MDOF structures through the Π theorem:

$$\left.\begin{matrix} X_{\max} \\ \dot{X}_{\max} \end{matrix}\right\} = f\left(m_a, m_b, K_a, \mu, u_{ya}, u_{yb}, \xi, \alpha, \overline{\omega}, e, d, a_p, \omega_p\right). \tag{10}$$

From equation (10), the equation contains a total of 13 variables and only three basic dimensions, mass [M], length [L], and time [T], are involved. On the basis of the Π theorem, the number of independent dimensionless Π-parameters can be reduced as (13 variables)-(3 reference dimensions) = 10 Π-parameters. In the former section (Section 1.2), the mass m_b of the right MDOF structure, amplitude a_p, and angular frequency ω_p of the sinusoidal excitation are chosen as the basic variables. The equations of motion of the two inelastic MDOF structures are dimensionless, and the modified expression of equation (10) is

$$\left.\begin{matrix} \dfrac{X_{\max}\omega_p^2}{a_p} \\ \dfrac{\dot{X}_{\max}\omega_p}{a_p} \end{matrix}\right\} = \phi\left(\frac{m_a}{m_b}, \frac{K_a}{m_b\omega_p^2}, \mu, \frac{u_{ya}\omega_p^2}{a_p}, \frac{u_{yb}\omega_p^2}{a_p}, \xi, \alpha, \frac{\overline{\omega}}{\omega_p}, e, \frac{d\omega_p^2}{a_p}\right). \tag{11}$$

Also,

$$\begin{cases} \Pi_u = \dfrac{X_{\max}\omega_p^2}{a_p}, \\ \Pi_v = \dfrac{\dot{X}_{\max}\omega_p}{a_p}, \\ \Pi_m = \dfrac{m_1}{m_2}, \\ \Pi_{\omega 1} = \dfrac{\omega_1}{\omega_p}, \\ \Pi_{\omega 2} = \dfrac{\omega_2}{\omega_p}, \\ \Pi_{uy1} = \dfrac{u_{y1}\omega_p^2}{a_p}, \\ \Pi_{uy2} = \dfrac{u_{y2}\omega_p^2}{a_p}, \\ \Pi_\xi = \xi, \\ \Pi_\alpha = \alpha, \\ \Pi_{\omega\mathrm{con}} = \dfrac{\overline{\omega}}{\omega_p}, \\ \Pi_e = e, \Pi_d = \dfrac{d\omega_p^2}{a_p}. \end{cases} \tag{12}$$

Equation (11) can be rewritten as

$$\left.\begin{matrix} \Pi_u \\ \Pi_v \end{matrix}\right\} = \phi\left(\Pi_m, \Pi_{\omega 1}, \Pi_{\omega 2}, \Pi_{uy1}, \Pi_{uy2}, \Pi_\xi, \Pi_\alpha, \Pi_{\omega\mathrm{con}}, \Pi_e, \Pi_d\right), \tag{13}$$

where $\Pi_m = m_a/m_b$ is the mass ratio of the left to the right structure. $\Pi_k = (K_a/m_b\omega_p^2)$ is the dimensionless stiffness story of the left structure. $\Pi_{uyi} = u_{yi}\omega_p^2/a_p\,(i = a, b)$ is the ratio of the yield displacement u_{yi} to the excitation energy scale $l_e = a_p/\omega_p^2$ of each structure, that is, the dimensionless

yield displacement. Π_{uyi} and Π_{α} are the parameters characterizing the structural inelasticity. Furthermore, $\Pi_{\omega\,\mathrm{con}}$ and Π_d with Π_e are the parameters that characterize the pounding properties; among them, the ratio of the angular frequency of the contact element to the sinusoidal excitation is represented by $\Pi_{\omega\mathrm{con}} = (\overline{\omega}/\omega_p)$.

3. Numerical Solution of the Pounding Response of Adjacent Inelastic MDOF Structures

Equation (7a) is solved by using the Newmark-β method [25], in which the parameters are taken as $\gamma = 1/2$, $\beta = 1/4$. The time step is $\Delta\tau = 0.001$. The following dimensionless Π-parameters are used

$$\begin{aligned}
\Pi_m &= (m_a/m_b) = 0.25,\\
\Pi_k &= 5,\\
\Pi_\mu &= 10,\\
\Pi_{uya} &= 0.1,\\
\Pi_{uyb} &= 0.06,\\
\Pi_\xi &= 0.05,\\
\Pi_\alpha &= 0.1,\\
\Pi_{\omega\mathrm{con}} &= 65,\\
\Pi_e &= 0.4,\\
\Pi_d &= 0.5.
\end{aligned} \tag{14}$$

Through the MATLAB program, the numerical procedure has been realized. The analysis results of the displacement, pounding force, and velocity histories of the adjacent inelastic MDOF structures are shown in Figures 3–5 for the first story, the second story, and the third story, respectively. The displacement histories, velocity histories, and pounding force contrast curve for the third story of the two adjacent structures with the improved Kelvin model and Kelvin model considering pounding and nonpounding are shown in Figure 6.

Figures 3(a)–5(a) show that the curves corresponding to the left and right structures of the three stories have 8 coincidences, indicating that, during the excitation time $\tau = 0 \sim 50$ s, there were 8 collisions on each story. Additionally, 8 mutations arise in the pounding force histories shown in Figures 3(b)–5(b), which are consistent with the previous conclusions. Moreover, the magnitude of the pounding force recorded on each story is not much different. Therefore, it is unreasonable to consider the collision effect of the highest story if the collision model is simplified to ignore the collision effect of the remaining stories. In addition, the left structure with a small mass and stiffness is obviously suppressed in positive displacement after pounding and produces a larger negative displacement than the right structure; however, the peak displacement response of the left structure is significantly reduced compared to the nonpounding situation (as shown in Figures 3(a)–5(a)). The right structure with a larger mass and stiffness has a significantly increased displacement response after pounding.

Moreover, pounding has an obvious influence on the velocity response of adjacent structures, as shown in Figures 3(c)–5(c). The velocity histories of the two structures change dramatically after pounding, and the velocity response of the left structure changes from positive to negative while the velocity response of the right structure increases. Therefore, the instantaneous sharp change in the velocity response is one of the basic features of the collision of the structure.

The hysteresis curve of each story of the two adjacent inelastic structures under the parameters of this paper is given in Figures 3(d)–5(d) and Figures 3(e)–5(e). The figures show that the first and the second story of both structures are entering the plastic stage; however, the hysteretic curve of the third story structure is a straight line, indicating that it is already in the elastic stage.

In addition to the velocity histories, Figure 6 compares the collision force history of the third story that is obtained by the improved Kelvin model and the Kelvin model. From the velocity histories of both structures, the histories of the two pounding models basically coincide, which proves the correctness of the numerical solution method obtained by the improved Kelvin model. From the time history curves of pounding force obtained using the two pounding models shown in Figure 6(c), a negative pulling force occurs during the rebound phase when the pounding process is simulated by using the Kelvin model. However, there exists no negative pulling force when the modified Kelvin model is used to simulate the pounding process. This is also a good display of the velocity histories as shown in Figures 6(a) and 6(b). In the enlarged part of the two figures, due to the tension of the Kelvin model during the rebound phase, the velocity histories will decrease during the pounding rebound phase, but this is not the case with the velocity histories obtained by the improved Kelvin model. Therefore, the improved Kelvin model can overcome the shortcomings of the Kelvin model, represent the real physical phenomena, and reflect the physical laws.

4. Shaking Table Pounding Test of Adjacent Multistory Structures

To further verify the correctness and effectiveness of the theoretical method proposed in this paper, the shaking table pounding test of adjacent four-story and three-story steel frame structure models is carried out, and the experimental model is numerically simulated such that the test results are dimensionless after being compared to the numerical simulation results.

4.1. Design of the Scale Structure Model. The experiment is based on the existing shaking table set up at Huazhong University of Science and Technology (HUST). The plan dimension of the shaking table is $4\,\mathrm{m} \times 4\,\mathrm{m}$, and the maximum load is $1.5 \times 10^4\,\mathrm{kg}$. According to the size of the shaking table and the similarity theorem, the geometric similarity ratio of the shaking table test S_l is 1 : 16.

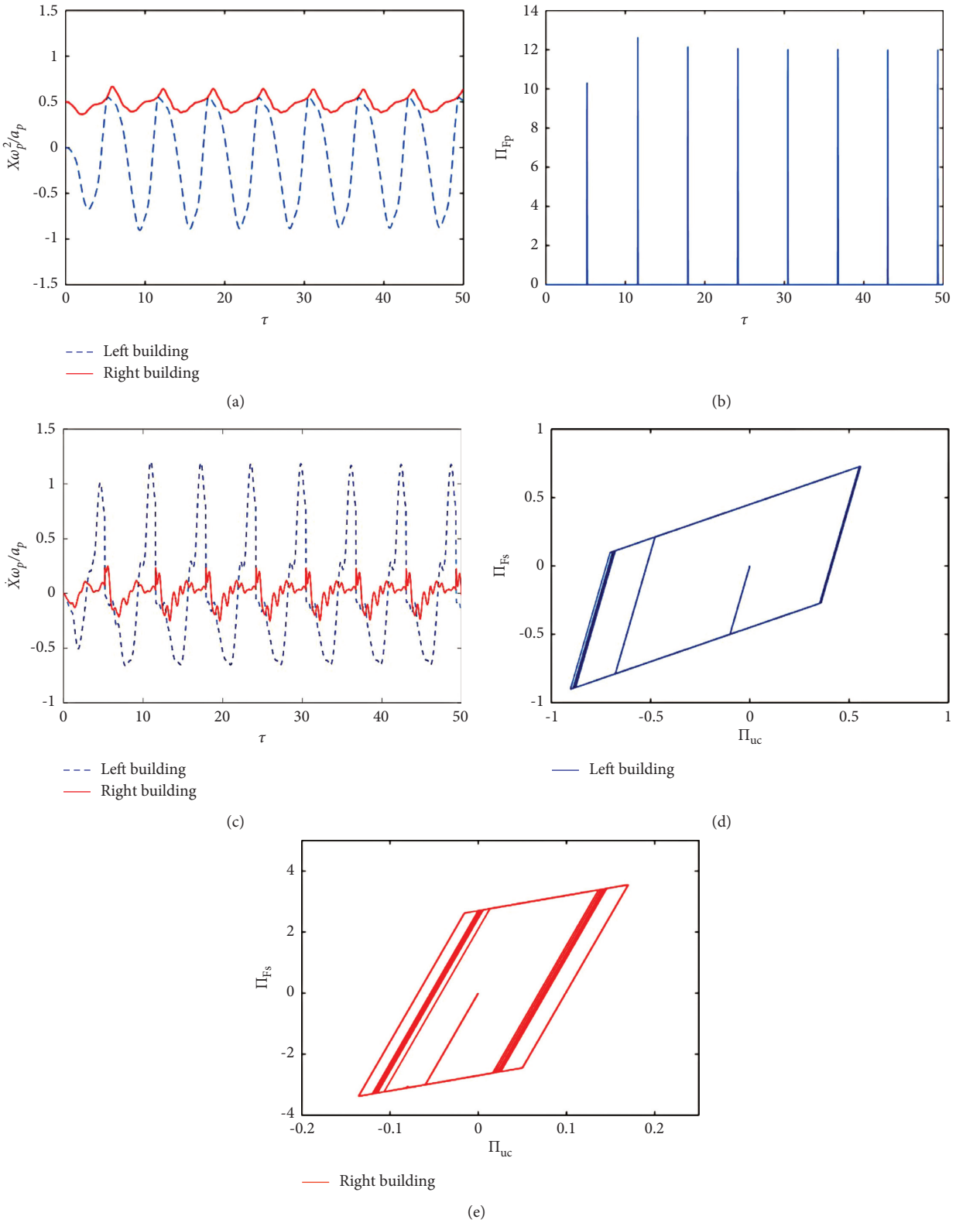

Figure 3: Displacement, velocity, pounding force histories, and hysteresis curves for the first story of adjacent buildings. (a) Displacement histories. (b) Pounding force histories. (c) Velocity histories. (d) Hysteresis curve of the left structure. (e) Hysteresis curve of the right structure.

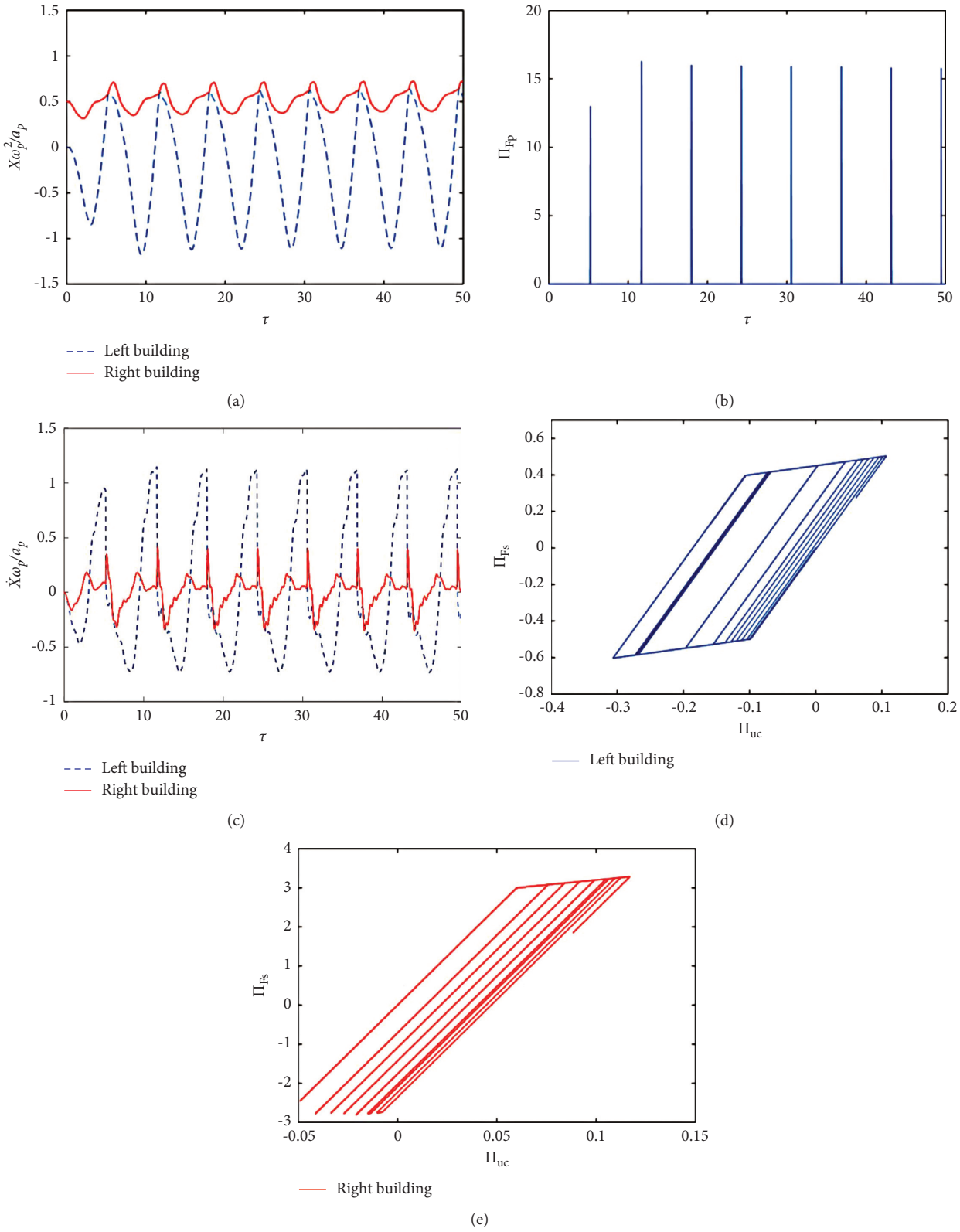

Figure 4: Displacement, velocity, pounding force histories, and hysteresis curves for the second story of adjacent buildings. (a) Displacement histories. (b) Pounding histories. (c) Velocity histories. (d) Hysteresis curve of the left structure. (e) Hysteresis curve of the right structure.

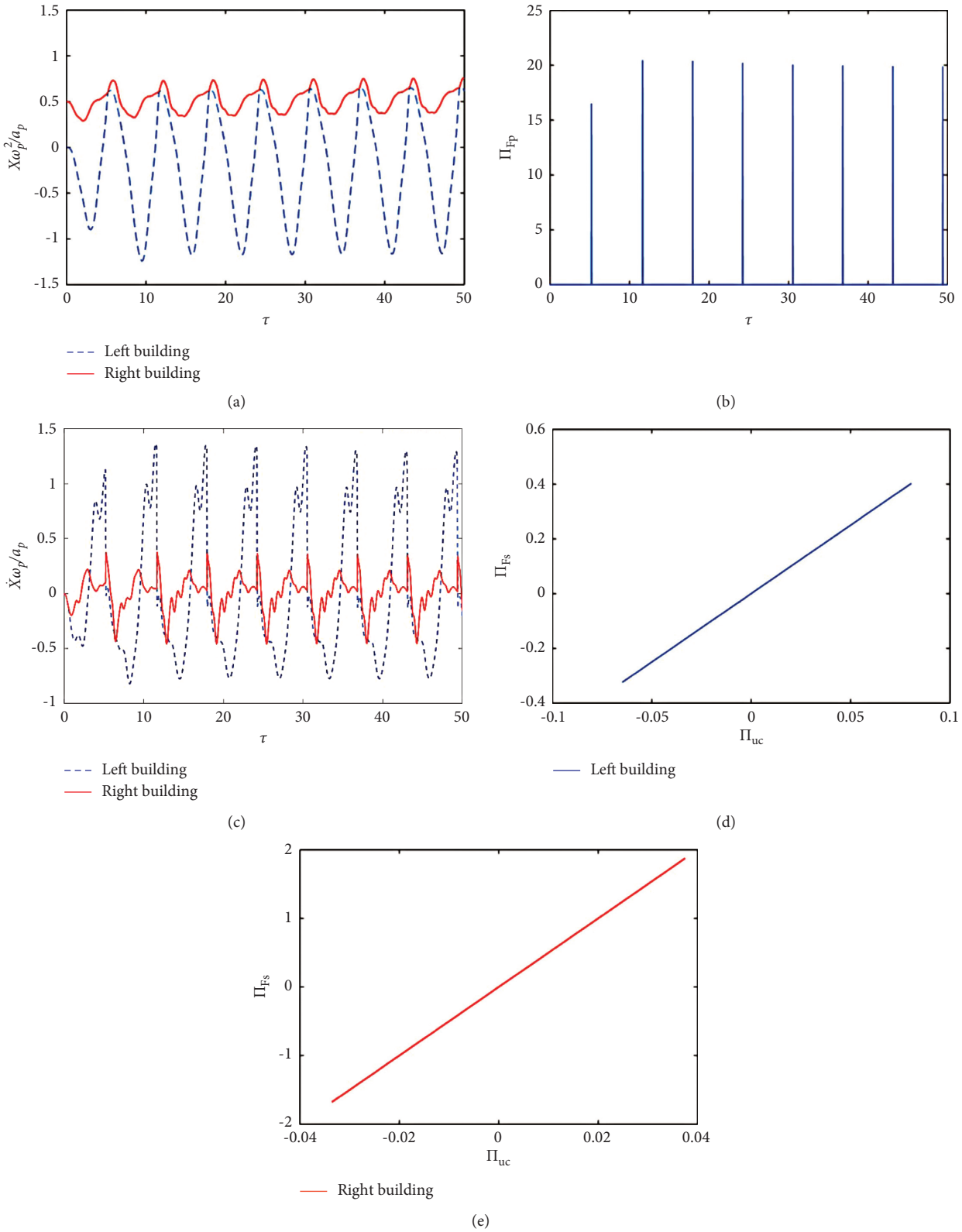

FIGURE 5: Displacement, velocity, pounding force histories, and hysteresis curves for the third story of adjacent buildings. (a) Displacement histories. (b) Pounding histories. (c) Velocity histories. (d) Hysteresis curve of the left structure. (e) Hysteresis curve of the right structure.

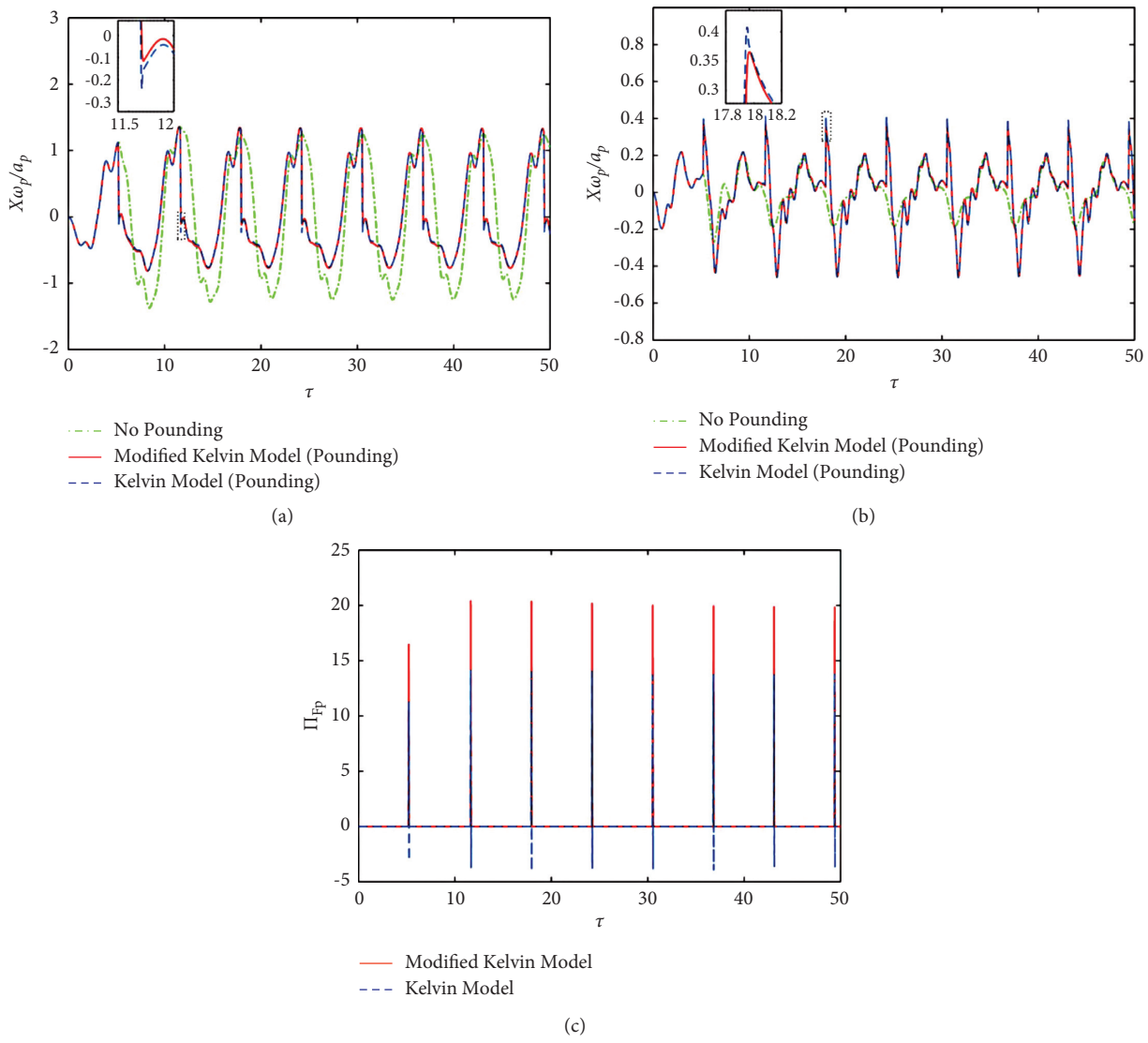

FIGURE 6: Two structures using the modified Kelvin model and the Kelvin model to consider the pounding of the third story. (a) Velocity histories of the left structure. (b) Velocity histories of the right structure. (c) Pounding force comparison curve.

Considering the convenience of material selection, the scale model structure of the test will be modeled with the same structural material (Q235 steel) as the original model structure. Therefore, the scaled model has the same density and modulus of elasticity as the original model, where $S_E = S_\rho = 1$. According to the similarity criterion, the similarity relations for the parameters of the scale model can be determined, as shown in Table 1.

The geometric similarity ratio can be determined according to Table 1, and the structural dimensions of the two adjacent multistory steel frame scaling models are determined as follows:

Structure A: four-story structure, 1.6 m × 0.8 m, story height 0.8 m

Structure B: three-story structure, 1.6 m × 0.8 m, story height 0.8 m

To ensure that the design of the original model conforms to the actual situation, the standard value of the constant load of the prototype structure story (excluding floor self-weight) is 1.5 kN/m^2. According to the Code for Load of Building Structures (GB50009-2012), the standard value for the story live load is 2.0 kN/m^2. Considering that the first story of the experimental scale model simulates four stories of the original structure, the standard value of the constant load of the story and the live load of the story can be determined as 6.0 kN/m^2 and 8.0 kN/m^2, respectively. Thus, through calculation, the additional mass of the top story is 0.32 t for scale structures A and B and 1.3 t for the other

Table 1: Similarity ratios of the test models.

Physical quantity	Symbol	Dimension	Similarity coefficient
Length	S_l	L	1/16
Modulus of elasticity	S_E	$ML^{-1}T^{-2}$	1
Rigidity	S_k	MT^{-2}	1/16
Acceleration	S_a	L/T^2	1
Time	S_T	T	1/4
Speed	S_v	L/T	1/4
Displacement	S_x	L	1/16
Quality (the self-weight and additional mass)	S_m	M	1/256

Table 2: The main components of the scale model for the test.

Component types	Section/mm	Length/m
Column 1	L110 × 8	0.8
Beam 1	L110 × 12	1.38
Beam 2	L110 × 12	0.58

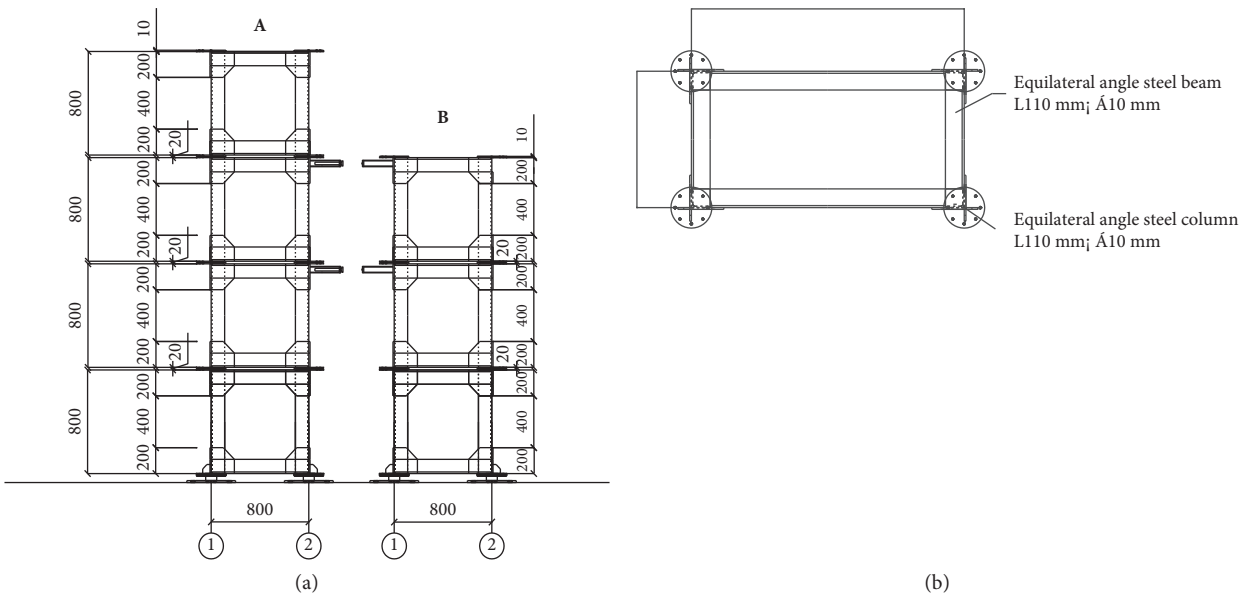

Figure 7: Detailed dimension diagram of the scale model. (a) Elevation of the scale model. (b) Top view of the scale model.

stories. A C20 prefabricated concrete slab is used as an additional mass of the story in this test.

According to the calculation from the similarity theory, the detailed information of the various components of the scale model is shown in Table 2. Figure 7 shows detailed dimensions of the scale model, and Figure 8 shows the test model.

Since the test model is bolted according to the fixed holes reserved on the shaking table, the distance between the adjacent steel frames is constant during the test; however, the neighboring structures cannot collide during the test because of the large distance between the two reserved holes. Therefore, a scalable pounding element is designed that consists of an impacting and receiving end and is located on the second and third stories of the adjacent steel frames, respectively. To ensure that point-to-surface pounding occurs between the impacting end and the receiving end, a section of an 8 mm thick steel rod is welded at the center of the front end of the receiver. The detailed designs of the pounding end and the actual pounding end model are shown in Figure 9.

4.2. Design of the Test Scheme

4.2.1. Scheme of Measurement. The shaking table test is mainly used to study the pounding reaction between adjacent steel frames. The main recorded data include the displacement and acceleration responses of each story and the shaking table. Therefore, the IMC and DH5922 dynamic acquisition instruments are selected for data acquisition, where the IMC dynamic acquisition instrument is used to collect the displacement and the DH5922 dynamic acquisition instrument is used to collect the acceleration. The arrangement of the displacement and acceleration measurement points is shown in Figure 10.

(a) (b)

Figure 8: Model diagram of the test. (a) Elevation of the test model. (b) Top view of the test model.

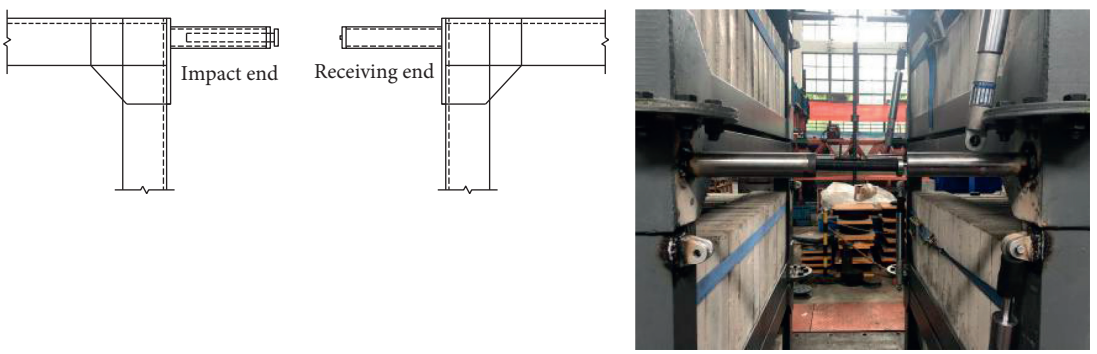

(a) (b)

Figure 9: Pounding end design. (a) Diagram of the pounding element. (b) Charts of impact elements for the test models.

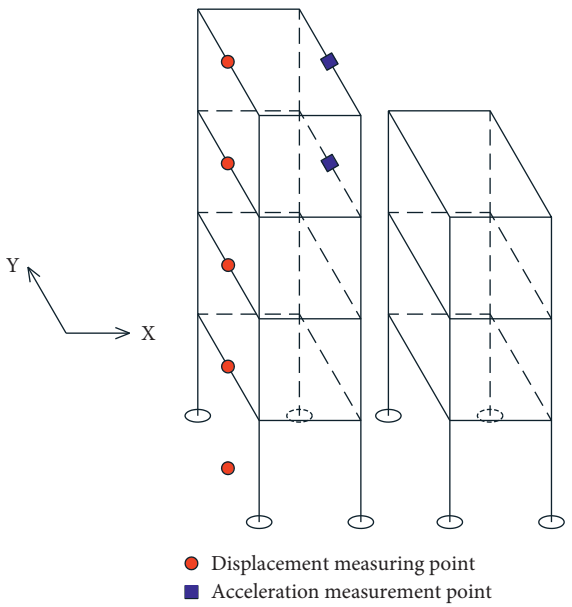

Figure 10: Layout of the measuring points.

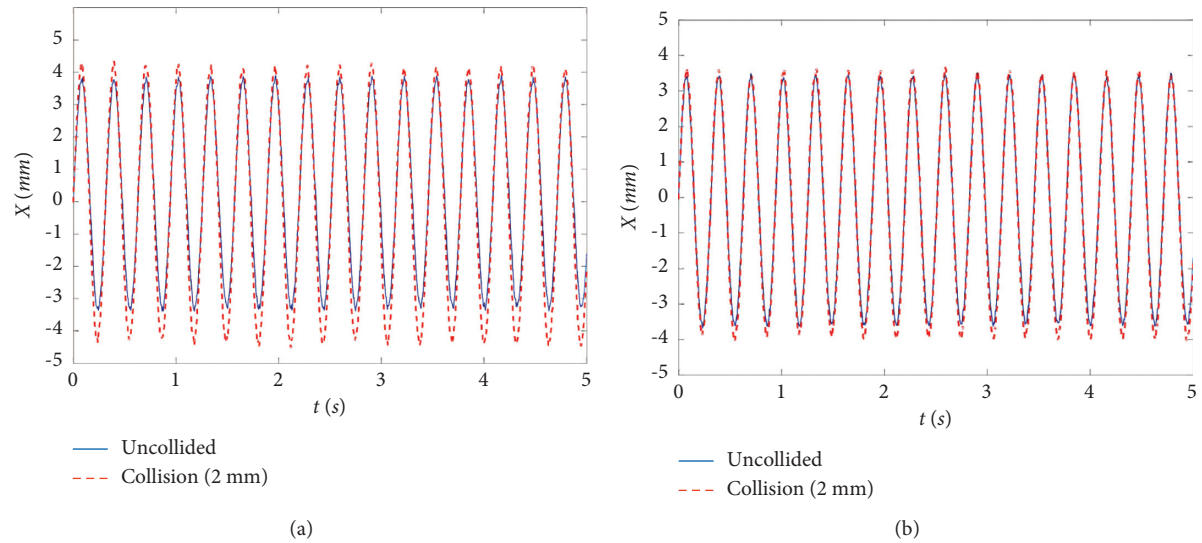

Figure 11: Relative displacement histories of the top and third story of structure A under pounding and nonpounding loading. (a) Histories of the relative displacement of the top story. (b) Histories of the relative displacement of the third story.

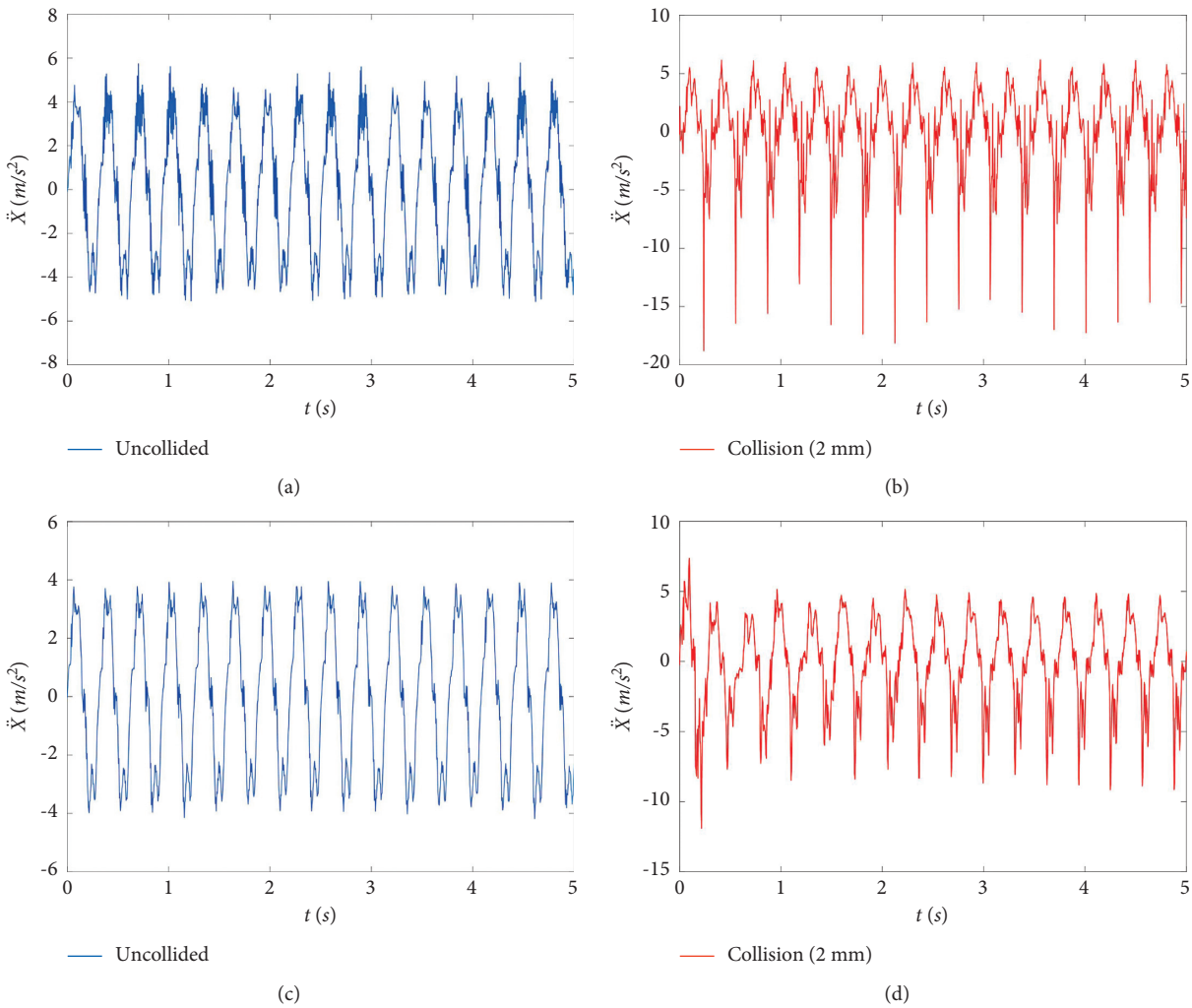

Figure 12: Acceleration histories of the top and third story of structure A under pounding and nonpounding loading. (a, b) Acceleration response histories of the top structure. (c, d) Acceleration response histories of the third story structure.

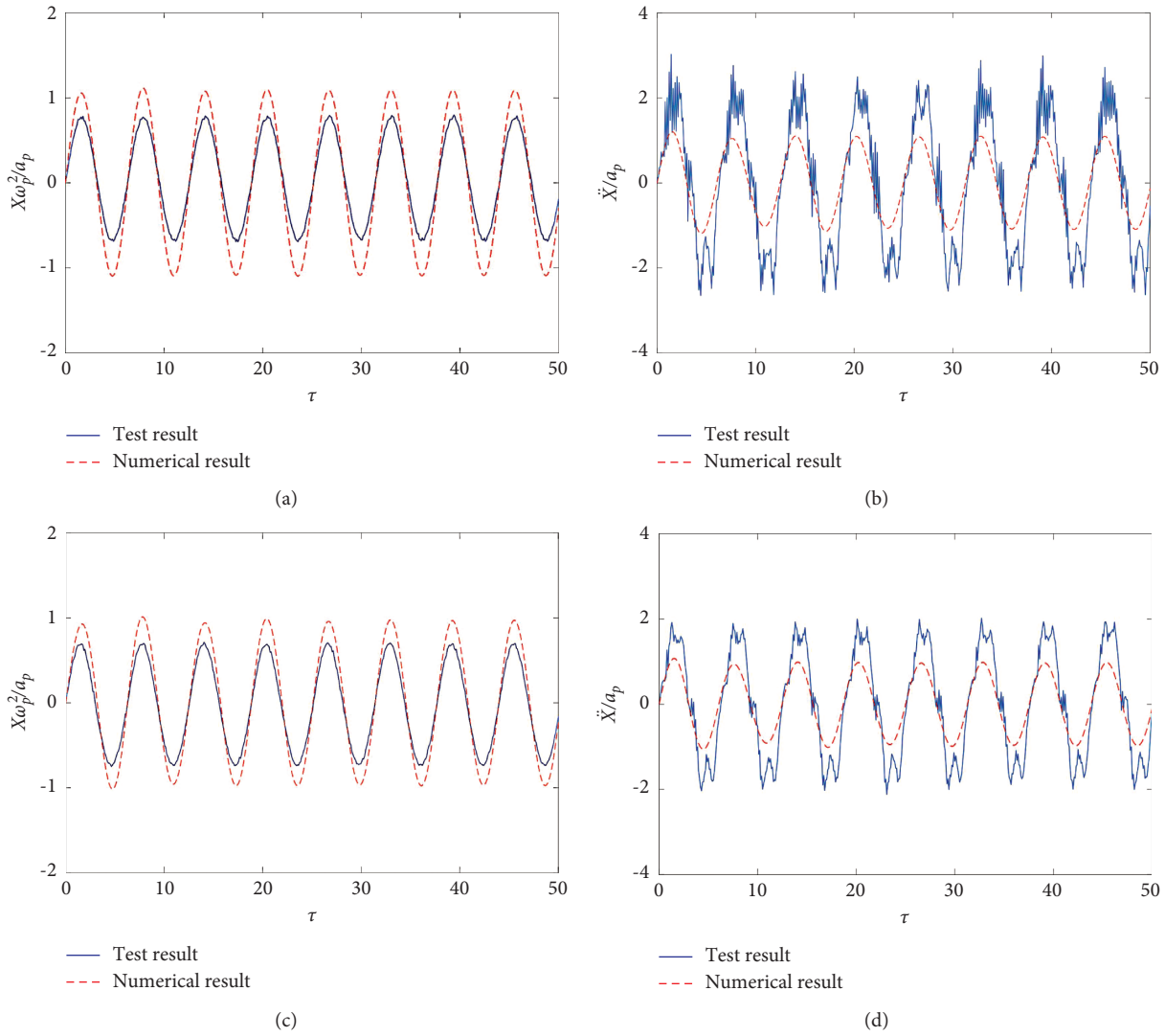

FIGURE 13: Displacement and acceleration histories of the top and third floors of the four-story steel frame structures without pounding. (a) Dimensionless displacement histories of the top floor. (b) Dimensionless acceleration histories of the top floor. (c) Dimensionless displacement histories of the third floor. (d) Dimensionless acceleration histories of the third floor.

There are two test conditions selected: no pounding and pounding with an adjacent spacing of 2 mm. Taking the case of no pounding as an example, the loading process of the whole test is as follows: first, the white noise is used to sweep the frequency of the two steel frames to check whether the dynamic characteristics of the structure have changed. Then, a sinusoidal wave (the frequency of the sinusoidal wave is 20 rad/s) with a peak acceleration of 0.2 g being selected for loading, and finally, a white noise sweep is performed. To date, the first loading condition has been completed.

4.3. Results of the Test. Figure 11 shows the relative displacement response histories of the top and third stories of a four-story steel frame structure with or without pounding (spacing is 2 mm) (obtained by subtracting the measured displacement response histories data of the floor from the corresponding displacement response histories data of the shaking table).

As shown in Figure 11, the actual displacement of the top and third stories are larger for the pounding case than that of the nonpounding case, which means that the pounding loading will amplify the displacement response of the structure.

Figure 12 shows the acceleration response histories of the top and third stories of the four-story steel frame structure without and with pounding (spacing at 2 mm). The acceleration response of the top and third stories exhibits obvious pulses during pounding, and the acceleration of the top and third stories is much greater than that of the nonpounding case, indicating that the pounding loading also enlarges the acceleration response of the structure.

4.4. Comparison of the Numerical Simulation Results with the Experimental Model Results. The four-story steel frame model and the three-story steel frame model are simplified into the lumped mass model, where the mass of each story is

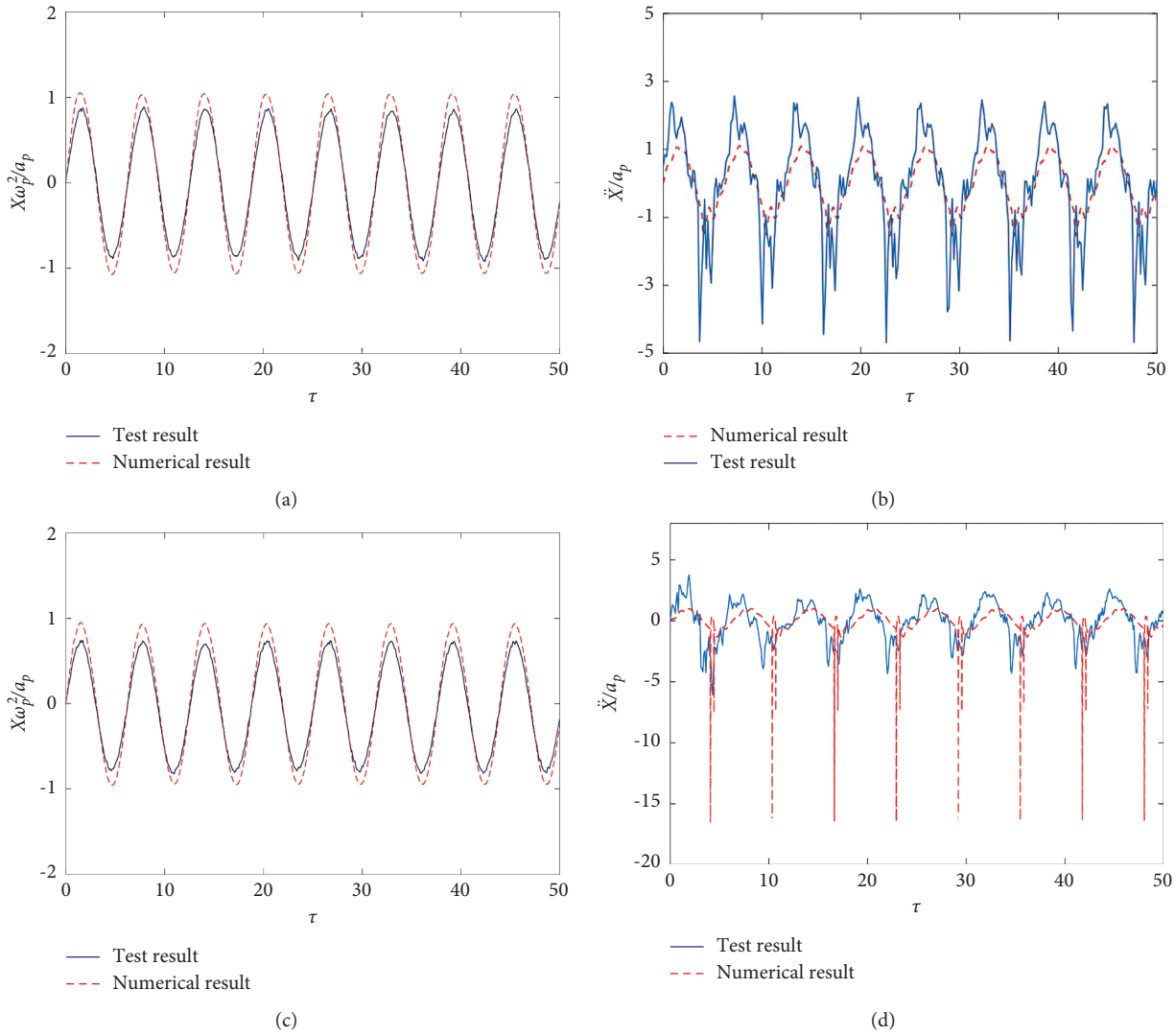

Figure 14: Displacement and acceleration histories of the top and third floors of the four-story steel frame structures with pounding. (a) Dimensionless displacement histories of the top floor. (b) Dimensionless acceleration histories of the top floor. (c) Dimensionless displacement histories of the third floor. (d) Dimensionless acceleration histories of the third floor.

1.7 t and it is assumed that the lateral stiffness of each story is equal. Through analysis and calculation, the story stiffness is obtained, and the results of the white noise frequency sweep confirm that the structure is in an elastic state during the whole test process.

Dimensionless parameters for the numerical calculation are obtained from the dimensionless test parameters, $\Pi_m = 1$, $\Pi_k = 17.5$, $\Pi_\mu = 1$, $\Pi_\xi = 0.05$, $\Pi_{\omega\text{con}} = 65$, $\Pi_e = 0.4$, $\Pi_d = 0.41$. Figures 13 and 14 show that by numerically solving the problem using MATLAB, comparative analysis of the obtained results with the dimensionless measured results.

Figure 13 shows the displacement and acceleration histories of the top and third floors of the four-story steel frame structure without pounding, and the comparison curves between the experimental and numerical results under the action of a sinusoidal wave with a peak acceleration of 0.2 g. The numerical results of the displacement response of the top and third floors are slightly larger than the experimental results, while the numerical results of the acceleration response are slightly smaller than the experimental results. This may be due to the fact that the actual structure is reduced to a centralized mass model, and the errors generated during the simplification process are caused. However, the frequency and waveform of the numerical results are consistent with the experimental results which can prove the validity and rationality of the mathematical model derived above.

Figure 14 shows the comparison curves of the test results and numerical results of the displacement and acceleration histories of the top and third floors of the four-story steel frame structure with pounding. The numerical results of the displacement response of the top and third floors are broadly consistent with the results of the experiment, verifying that the method is correct. Due to the collision effect, the acceleration response of the structure has obvious pulses, but

the number of collisions obtained by the numerical solution is more than the number recorded by the experiment as shown in Figure 4(d). The numerical solution of the acceleration response of the top floor is smaller than the test result and the numerical solution of the acceleration response of the third floor is greater than the test result. The reason for this difference may be that the numerical model simplifies the experimental model into a lumped mass model, resulting in errors in the process of simplification.

5. Conclusion

In this paper, the dimensional analysis and the contact element method are combined to study the pounding response of adjacent nonlinear MDOF structures under simplified earthquake loadings. The improved Kelvin model is used to simulate the force and deformation of the two structures in the process of collision and contact, and the bilinear interstory resistance model is used to simulate the inelastic characteristics of the structure. Two inelastic dimensionless pounding force expressions and dimensionless motion equations of the MDOF structures are deduced. When dimensionless parameters Π are adopted, the number of variables affecting the pounding response of the two inelastic MDOF structures is reduced from 13 to 10. Moreover, the pounding law is clearly exhibited, and the contact deformation process is also presented. Under the selected parameters, the displacement, velocity, pounding force, and hysteretic curve of each story of the adjacent MDOF structures are predicted by the improved Kelvin model. The correctness of the proposed pounding response analysis method and the advantage of the improved Kelvin model are verified by comparing the pounding response obtained by the improved Kelvin model and that from the Kelvin model. Besides, the shaking table tests are carried out on adjacent four-story and three-story steel frame structures, and comparing the results from the experiment with the corresponding results from numerical simulations obtained by the MATLAB program further confirms the validity and effectiveness of the proposed pounding response analysis method.

Data Availability

Some data, models, or codes that support the findings of this study are available from the corresponding author upon reasonable request.

Conflicts of Interest

The authors declare that there are no conflicts of interest regarding the publication of this paper.

Acknowledgments

The authors are grateful to the National Nature Science Foundation of China (Grant no. 52078395), the Open Research Fund of State Key Laboratory of Geomechanics and Geotechnical Engineering, Institute of Rock and Soil Mechanics, Chinese Academy of Sciences (Grant no. Z018013) and the Open Research Fund of State Key Laboratory of Coastal and Offshore Engineering, Dalian University of Technology (Grant no. LP1920). The authors also very much appreciate the State Key Lab of Subtropical Building Science, South China University of Technology (Grant no. 2019ZB20), and the Key Laboratory of Urban Security and Disaster Engineering of Ministry of Education, Beijing University of Technology.

References

[1] P. Zhu, M. Abe, and Y. Fujino, "Evaluation of pounding countermeasures and serviceability of elevated bridges during seismic excitation using 3D modeling," *Earthquake Engineering & Structural Dynamics*, vol. 33, no. 5, pp. 591–609, 2010.

[2] C.-J. Wang and M.-H. Shih, "Performance study of a bridge involving sliding decks and pounded abutment during a violent earthquake," *Engineering Structures*, vol. 29, no. 5, pp. 802–812, 2007.

[3] C.-J. Wang, "Failure study of a bridge subjected to pounding and sliding under severe ground motions," *International Journal of Impact Engineering*, vol. 34, no. 2, pp. 216–231, 2007.

[4] F. D. Ruiz Julian, T. Hayashikawa, and T. Obata, "Seismic performance of isolated curved steel viaducts equipped with deck unseating prevention cable restrainers," *Journal of Constructional Steel Research*, vol. 63, no. 2, pp. 237–253, 2007.

[5] E. Rosenblueth and R. Meli, "The 1985 earthquake: causes and effects in Mexico City[J]," *Concrete International*, vol. 8, no. 5, pp. 23–34, 1986.

[6] F. Naeim, M. Lew, S. C. Huang, H. K. Lam, and L. D. Carpenter, "The performance of tscct," *The Structural Design of Tall Buildings*, vol. 9, no. 2, pp. 137–160, 2000.

[7] Y. Ren, R. Wen, H. Yamanaka, and T. Kashima, "Site effects by generalized inversion technique using strong motion recordings of the 2008 Wenchuan earthquake," *Earthquake Engineering and Engineering Vibration*, vol. 12, no. 2, pp. 165–184, 2013.

[8] C. Y. Bai, Q. Q. Si, and X. Lei, "Identification of seismic type of 2017 Iraq M_W7.3 earthquake and analysis of its post-quake trend," *Chinese Journal of Geophysics*, vol. 61, no. 2, pp. 616–624, 2018, in Chinese.

[9] B. F. Maison and K. Kasai, "Analysis for a type of structural pounding," *Journal of Structural Engineering*, vol. 116, no. 4, pp. 957–977, 1990.

[10] S. A. Anagnostopoulos and K. V. Spiliopoulos, "An investigation of earthquake induced pounding between adjacent buildings," *Earthquake Engineering & Structural Dynamics*, vol. 21, no. 4, pp. 289–302, 1992.

[11] S. Mahmoud and R. Jankowski, "Elastic and inelastic multistorey buildings under earthquake excitation with the effect of pounding," *Journal of Applied Sciences*, vol. 9, no. 18, pp. 3250–3262, 2009.

[12] R. Jankowski, "Earthquake-induced pounding between equal height buildings with substantially different dynamic properties," *Engineering Structures*, vol. 30, no. 10, pp. 2818–2829, 2008.

[13] C. H. Zhai, S. Jiang, and Z. Q. Chen, "Dimensional analysis of the pounding response of an oscillator considering contact duration," *Journal of Engineering Mechanics*, vol. 141, Article ID 04014138, 2015.

[14] M. Levin, *Chapter 2 - Dimensional Analysis*, Elsevier, Amsterdam, Netherlands, 2016.
[15] N. Makris and C. J. Black, "Dimensional analysis of rigid-plastic and e structures under pulse-type excitations," *Journal of Engineering Mechanics*, vol. 130, no. 9, pp. 1006–1018, 2004.
[16] N. Makris and C. J. Black, "Dimensional analysis of bilinear oscillators under pulse-type excitations," *Journal of Engineering Mechanics*, vol. 130, no. 9, pp. 1019–1031, 2004.
[17] J. Zhang and Y. Tang, "Dimensional analysis of structures with translating and rocking foundations under near-fault ground motions," *Soil Dynamics and Earthquake Engineering*, vol. 29, no. 10, pp. 1330–1346, 2009.
[18] E. Dimitrakopoulos, N. Makris, and A. J. Kappos, "Dimensional analysis of the earthquake-induced pounding between adjacent structures," *Earthquake Engineering & Structural Dynamics*, vol. 38, no. 7, pp. 867–886, 2009.
[19] E. Dimitrakopoulos, A. J. Kappos, and N. Makris, "Dimensional analysis of yielding and pounding structures for records without distinct pulses," *Soil Dynamics and Earthquake Engineering*, vol. 29, no. 7, pp. 1170–1180, 2009.
[20] E. Dimitrakopoulos, N. Makris, and A. J. Kappos, "Dimensional analysis of the earthquake response of a pounding oscillator," *Journal of Engineering Mechanics*, vol. 136, no. 3, pp. 299–310, 2010.
[21] Q. Wu, T. Wang, H. Ge, and H. Zhu, "Dimensional analysis of pounding response of an oscillator based on modified Kelvin pounding model," *Journal of Aerospace Engineering*, vol. 32, no. 4, Article ID 04019039, 2019.
[22] K. Ye, L. Li, and H. Zhu, "A modified Kelvin impact model for pounding simulation of base-isolated building with adjacent structures," *Earthquake Engineering and Engineering Vibration*, vol. 8, no. 3, pp. 433–446, 2009.
[23] J. Penizen, "Dynamic response of elasto-plastic frames," *Journal of Structural Division, ASCE*, vol. 88, no. ST7, pp. 1322–1340, 1962.
[24] S. Jiang, "Dimensional analysis of earthquake-induced pounding between adjacent inelastic MDOF buildings," *Earthquake Engineering and Engineering Vibration*, vol. 14, no. 2, pp. 295–313, 2015.
[25] N. M. Newmark, "A method of computation for structural dynamics," *Journal of the Engineering Mechanics Division*, vol. 85, no. 3, pp. 67–94, 1959.